

Enhanced activation of interleukin-10 and AKT signaling in C5aR2 deficient mice is associated with protection from ischemia reperfusion injury induced inflammation and fibrosis

Anja Thorenz PhD^{1*}, Katja Hueper MD^{2*}, Christoph Schroeder PhD⁷, Lisa Dressler BSc⁷, Vijith Vijayan PhD⁹, Pooja Pradhan MSc⁹, Stephan Immenschuh MD⁹, Anne Jörns MD¹⁰, Frank Echtermeyer PhD¹¹, Christine Herzog PhD¹¹, Rongjun Chen PhD¹, Song Rong MD¹, Jan Hinrich Bräsen MD⁵, Cees van Kooten PhD⁸, Torsten Kirsch PhD¹, Christian Klemann MD⁶, Martin Meier PhD⁴, Andreas Klos MD³, Hermann Haller MD¹, Bennet Hensen MD^{2#}, Faikah Gueler MD^{1#}

Correspondence to:
Prof. Faikah Gueler,
Nephrology
Hannover Medical School,
Carl-Neuberg-Str.1, 30625 Hannover,
Tel: +49-511-532 3722, Fax: +49-511-552366
email: gueler.faikah@mh-hannover.de

¹Nephrology, ²Diagnostic and Interventional Radiology, ³Medical Microbiology and Hospital Epidemiology, ⁴Imaging Center of the Central Animal Facility, ⁵Pathology, ⁶Pediatric surgery, ⁹Transfusion Medicine, ¹⁰Clinical Biochemistry, ¹¹Department of Anesthesiology and Intensive Care Medicine, Hannover Medical School, Hannover, Germany

⁷Sciomics GmbH, Heidelberg, Germany

⁸ Nephrology, Leiden University Medical Center (LUMC), Netherlands

*AT and KH contributed equally

#BH and FG contributed equally

Abstract word count: 215

figures: 7

word count: 4,300 words

Head line: C5aR2 in IRI

Severe ischemia reperfusion injury (IRI) results in rapid complement activation, acute kidney injury and progressive renal fibrosis. Little is known about the roles of the C5aR1 and C5aR2 complement receptors in IRI. In this study C5aR1^{-/-} and C5aR2^{-/-} mice were compared to wild type (WT) in a renal IRI model leading to renal fibrosis.

We investigated C5a receptor expression, kidney morphology, inflammation, and fibrosis in different mouse strains 1, 7 and 21 days after IRI. Renal perfusion was evaluated by functional magnetic resonance imaging (fMRI). Protein abundance and phosphorylation were assessed with high content antibody microarrays and Western blotting.

C5aR1 and C5aR2 increased in damaged tubuli and even more in infiltrating leukocytes after IRI in WT mice. C5aR1^{-/-} and C5aR2^{-/-} animals developed less IRI-induced inflammation and showed better renal perfusion than WT mice. C5aR2^{-/-} mice, in particular, had enhanced tubular and capillary regeneration with less renal fibrosis. IL-10 and AKT levels were especially high in C5aR2^{-/-} IRI kidneys. LPS caused bone marrow derived macrophages from C5aR2^{-/-} mice to release anti-inflammatory IL-10 and to express HO-1.

Our data suggest that C5aR1 and C5aR2 have overlapping actions following renal IRI in mice. C5aR2^{-/-} kidneys regenerate better than those in C5aR1^{-/-} mice after IRI. This is mediated, in part at least, by differential production of IL-10, HO-1 and AKT.

Keywords: ischemia reperfusion injury, complement, fibrosis, regeneration, IL-10, AKT, renal perfusion, HO-1

INTRODUCTION

The complement system modulates immune responses in a number of renal diseases including acute kidney injury (AKI)^{1,2,3}, atypical hemolytic uremic syndrome (aHUS)⁴, glomerulonephritis^{5,6} and renal allograft rejection^{7,8}. The complement cascade can be activated by the classical, lectin or alternative pathway^{3,9} leading to formation of C3 convertase, which generates the membrane attack complex (MAC C5b-9) and anaphylatoxins C3a and C5a. C5a in particular is a key mediator of inflammatory kidney diseases^{3,10,11}. The two receptors, C5aR1 and C5aR2, orchestrate the inflammatory response. C5aR2 (formerly C5L2) is not coupled to G-proteins and was presumed to be a non-signalling decoy receptor regulating the function of C5aR1. Recently, C5aR2, but not C5aR1, was found to be required for mast cell adhesion and pro-inflammatory cytokine production in a model of allergic inflammation¹². Finally, two C5aR2-specific ligands (P32 and P59 based on the C-terminus of C5a) in human monocyte-derived macrophages have been identified¹³. Both C5a receptors are expressed on the surface of myeloid^{14,15}, dendritic¹⁶ and T-cells^{17,18,19}; and different expression patterns of C5aR1 and C5aR2 have been observed in human kidney transplant biopsies^{20,21}.

Cellular functions such as chemotaxis and activation of inflammatory leukocytes are modulated by C5aR activation. In models of delayed graft function and acute allograft rejection¹¹, hepatic²² IRI, and intestinal²³ IRI in mice, C5aR inhibitor treatment attenuated renal inflammation. C5aR deficiency has been linked to reduced leukocyte infiltration after myocardial infarctions²⁴ and in renal IRI²². However, these studies did not differentiate between the two C5aRs. In a recent study C5aR2^{-/-} mice had attenuated inflammation in a mild model of transient AKI²⁵. Our aim was to determine whether C5aR1^{-/-} and C5aR2^{-/-} mice develop different phenotypes in a model of unilateral severe IRI which progresses to renal fibrosis. This reflects the clinical situation in major surgeries where severe AKI can lead to chronic kidney disease (CKD)²⁶. The unilateral IRI-CKD model can be used to study disease progression in the clamped kidney because the contralateral organ allows the animal to survive. Inflammation and fibrosis were studied

longitudinally and compared to changes in renal perfusion assessed by fMRI. To learn more about the distinct functions of the two C5aRs, a proteomic approach was done which revealed changes in the levels and phosphorylation status of several proteins in the receptor deficient mice in response to IRI.

RESULTS

C5aR1 and C5aR2 are up-regulated in the IRI-CKD model

First, we characterized C5aR1 and C5aR2 expression in the model of IRI-induced renal fibrosis in WT mice. Within 24 hours, C5aR1 and C5aR2 mRNA levels increased significantly in IRI kidneys compared to contralateral control kidneys, which had transcript levels similar to those in kidneys from sham-operated mice. The mRNA levels of both C5aRs remained elevated in IRI kidneys for the whole observation period of 21 days (Fig. 1A and B). Activation of complement in EDTA plasma through the alternative (AP), classical (CP) and lectin (LP) pathway did not differ between mouse strains at baseline (Fig. 1C). C3 fragments as split products of complement activation were increased in all mouse strains at d1 and normalized around d7 (Fig 1D). Since no specific mouse antibodies for the two distinct mouse C5aRs are available, in situ hybridization on IRI WT kidneys was used to characterize the spatial and temporal distribution of C5aR1 and C5aR2 expressing cells. One day after IRI there was no evident increase of the mRNA in the tubule system for both receptors (Fig.1 E, I). Occasionally, immune cells expressing both receptors were detected in the perivascular space of large vessels. By d7, receptor-positive immune cells surrounded the vessels and tubules, and there were faint to moderate levels of C5aR1 and C5aR2 mRNAs (Fig. 1F and J) in the proximal tubules themselves. Twenty-one days after IRI, there was a marked increase in receptor mRNA staining in the proximal tubules (stars) and immune cells (arrows Fig. 1G, K). In contralateral WT control kidneys low-level expression of both receptors, C5aR1 (H)

and C5aR2 (L) in the proximal tubule was observed. As expected, knock out mice did not express the receptors that had been knocked out in their control kidneys.

Inflammation after IRI

Complement activation has been implicated in rapid attraction of myeloid cells to sites of injury. Gr-1⁺ neutrophils were found in the outer medulla one day after IRI and were replaced by F4/80⁺ macrophages on d7 (Fig. 2). WT and C5aR1^{-/-} IRI kidneys showed similar Gr-1⁺ neutrophil infiltration one day after IRI. Much less infiltration was observed in C5aR2^{-/-} IRI kidneys (Gr-1 scores: C5aR2^{-/-}: 1.2 ±0.16 vs WT: 2.6 ±0.125, ***p<0.001; C5aR2^{-/-} vs C5aR1^{-/-}: 2.25 ±0.144, **p<0.01, Fig. 2). At d7 F4/80⁺ macrophages were predominant in WT IRI kidneys. In C5aR1^{-/-} and especially in C5aR2^{-/-} IRI kidneys F4/80⁺ cells were markedly reduced (F4/80 scores: WT: 3 ±0 vs C5aR1^{-/-}: 2.3 ±0.14, ***p<0.001, WT vs C5aR2^{-/-}: 1.7±0.17, ***p<0.001; C5aR1^{-/-} vs C5aR2^{-/-} **p<0.01 Fig 2). We confirmed this finding by using flow cytometry to determine the number of CD11b⁺/F4/80⁺ cells per 100 mg of tissue (WT vs C5aR1^{-/-} *p<0.05; WT vs C5aR2^{-/-} **p<0.01, Fig 2). Control kidneys showed similar expression of myeloid cells in all mouse strains at baseline.

Inflammation compromises microcirculation; therefore, patency of peritubular capillaries (PTC) was investigated by lectin staining *in vivo*. There was normal patency at d1 (Fig. 2K) and a marked reduction in WT mice at d7. PTC patency was enhanced in C5aR1^{-/-} and even more in C5aR2^{-/-} IRI kidneys at d7 (Fig. 2N).

Cytokine expression and IL-10 and HO-1 signalling after IRI

Pro- and anti-inflammatory cytokines are important mediators of inflammation. Therefore, expression of IL-1 β and IL-6 mRNA in IRI kidneys was studied in the different mouse strains after IRI. At d1 the pro-inflammatory IL-1 β was significantly upregulated in WT kidneys but not in C5aR1^{-/-} and C5aR2^{-/-} IRI kidneys. The differences were less pronounced at d7 but

appeared to return again by d21 (Fig. 3A-C). IL-6 expression increased significantly in all mouse strains at d1 and remained elevated in WT mice at d7. C5aR1^{-/-} and C5aR2^{-/-} mice had less IL-6 expression at d7. At d21 no significant differences between the three mouse strains were present but IL-6 expression remained higher than in control kidneys (Fig. 3D-F). Based on antibody array results, the anti-inflammatory IL-10 protein was increased in C5aR2^{-/-} IRI kidneys on d1. To confirm this, IL-10 mRNA expression in C5aR2^{-/-}, C5aR1^{-/-}, and WT IRI kidneys was measured on days 1, 7 and 21 (Fig. 3G-I). Since IL-10 is a strong inducer of the anti-inflammatory hemoxygenase-1 (HO-1), this protein was studied using immunohistochemistry. HO-1 expression was up-regulated in the macrophages and proximal tubuli of C5aR2^{-/-} IRI kidneys on d1 (Fig. 3J-L). IL-10 is produced by myeloid cells and affects macrophage function. Therefore, bone marrow derived macrophages (BMM) were isolated from WT and C5aR2^{-/-} mice and stimulated with LPS. In the supernatant IL-10 protein abundance was much higher in C5aR2^{-/-} BMM than in WT cells (*p<0.05 Fig. 3M). In addition, HO-1 was significantly upregulated in C5aR2^{-/-} BMM (Fig. 3N). These cells had higher levels of CD206, a marker of anti-inflammatory macrophages (Fig. 3O).

Renal inflammation and integrity of the peritubular capillary network 21 days after IRI

Three weeks after IRI, >75% of the WT tubuli still showed signs of AKI. In C5aR1^{-/-} and even more in C5aR2^{-/-} IRI kidneys, AKI was reduced compared to WT (Fig. 4, first column). F4/80⁺ macrophages were the predominant infiltrating cell type 21 days after IRI, but a reduction in F4/80⁺ cells was seen in C5aR1^{-/-} IRI kidneys vs WT controls. An even greater decrease was found in kidneys from C5aR2^{-/-} mice. (F4/80 scores: WTvs C5aR1^{-/-} *p<0.05; WT vs C5aR2^{-/-} ***p<0.001 Fig. 4 middle column). Inflammation and AKI might cause loss of PTCs²⁷. To investigate the integrity of the capillary network after IRI *in vivo* lectin labelling was done 5 min prior to sacrifice. IRI WT kidneys showed loss of PTCs within 7 days (Fig. 2N), which increased towards d21 (Fig. 4 last column). The areas with the highest

accumulation of leukocytes showed the largest reduction of patent PTCs. In comparison, in the contralateral kidneys all PTCs were patent. C5aR2^{-/-} IRI kidneys had significantly enhanced numbers of patent PTCs at d7 compared to WT (WT: 45% \pm 2.89 vs C5aR2^{-/-}: 71% \pm 1.25, *** p <0.001). C5aR1^{-/-} IRI kidneys had also more patent PTCs on d7 than WT (C5aR1^{-/-}: 58% \pm 3.33 vs WT * p <0.05, vs C5aR2^{-/-} ** p <0.01, Fig. 2N). 21 days after IRI differences between WT and C5aR2^{-/-} kidneys were still high (WT: 59% \pm 1.64 vs C5aR1^{-/-}: 71% \pm 2.79, ** p <0.01; vs C5aR2^{-/-}: 79% \pm 2.39, *** p <0.001).

Renal perfusion impairment after IRI

Renal perfusion was studied *in vivo* with fMRI on d1, 7 and 21 (Fig. 5). All mouse strains showed similar impairment of renal perfusion at d1. Differences between strains became obvious at d7: C5aR1^{-/-} and C5aR2^{-/-} mice showed significantly better renal perfusion than WT mice (WT: 219 \pm 48 vs C5aR1^{-/-}: 352 \pm 19,5 ml/min/100g, * p <0.05; WT vs C5aR2^{-/-}: 351 \pm 45,4 ml/min/100g, * p <0.05, control kidneys: 943 \pm 41 ml/min/100g). Three weeks after IRI, renal perfusion was nearly normal in C5aR2^{-/-} mice and improved in C5aR1^{-/-} compared to WT mice (WT: 410 \pm 58 ml/min/100g vs C5aR1^{-/-}: 599 \pm 39 ml/min/100g, * p <0.05; WT vs C5aR2^{-/-}: 723 \pm 47 ml/min/100g, ** p <0.01). In C5aR2^{-/-} mice, this correlated with enhanced integrity of the PTC network and attenuated inflammation. Similarly, glomerular filtration rate (GFR) measured by inulin clearance after nephrectomy of the healthy contralateral kidney on d21 was significantly better in C5aR2^{-/-} than in WT IRI kidneys (WT: 11.4 \pm 2.32 μ l/min vs C5aR2^{-/-}: 49 \pm 5.1 μ l/min *** p <0.001, Fig. 5C). C5aR1^{-/-} mice also had improved GFR compared to WT mice (44 \pm 16 μ l/min, * p <0.05).

Renal fibrosis after IRI

Severe IRI causes progressive renal fibrosis with loss of kidney volume and renal function^{28,29}. Morphometric MRI studies revealed that the kidney volumes of WT mice were

reduced by 45% 21 days after IRI. Both C5aR1^{-/-} and C5aR2^{-/-} mice had smaller reductions in kidney volume suggesting better regeneration and less renal scarring (WT: 54.2 ±2.9% vs C5aR1^{-/-}: 58.6 ±2.7%; WT vs C5aR2^{-/-}: 65.9±1.3%, **p<0.01, Fig. 6).

WT and C5aR1^{-/-} mice showed similar interstitial collagen accumulation based on sirius red (SR) staining at d21. C5aR2^{-/-} mice were almost completely protected from interstitial fibrosis (SR⁺ tubulointerstitial area: WT: 32 ±2.82% vs C5aR1^{-/-}: 27 ±6.57%; WT vs C5aR2^{-/-}: 9 ±2.95% ***p<0.001, Fig. 6). These data show that C5aR1^{-/-} and C5aR2^{-/-} differed in their responses to IRI.

C5aR2^{-/-} mice had enhanced tubular epithelial cell proliferation

IRI causes cell death, but renal regeneration starts rapidly following injuries. Tubular epithelial cell proliferation was studied by Ki-67 staining. 24 hours after IRI, C5aR2^{-/-} kidneys showed significantly more Ki-67⁺ proliferating tubular epithelial cells than WT and C5aR1^{-/-} kidneys (C5aR2^{-/-}: 945 ±188 vs WT: 418 ±103, *p<0.05; C5aR2 vs C5aR1^{-/-}: 258 ±48, *p<0.05 Fig. 7A, B). Seven days after IRI significant differences were still present (C5aR2^{-/-} 926 ±35 vs WT 635 ±48 **p<0.01; C5aR2^{-/-} vs C5aR1^{-/-}: 493 ±37 ***p<0.001).

C5aR2^{-/-} IRI kidneys have enhanced AKT protein expression after IRI

To assess the molecular mechanisms responsible for improved regeneration in C5aR-deficient mice further, a high-content antibody microarray study^{30,31} was performed. The abundance and phosphorylation status of 897 proteins were determined 1 day after IRI. Significantly higher levels of AKT1 were detected in C5aR2^{-/-} compared to C5aR1^{-/-} IRI kidneys (logFC = 0.36, p = 0.014). To verify the array results on AKT1, Western blotting of p-AKT and AKT were performed and showed enhanced relative expression and phosphorylation of AKT in C5aR2^{-/-} IRI kidneys compared to WT a day after IRI (Fig. 7C-F). Collectively, the differentially expressed proteins and phospho proteins were compared by the pathway

analysis database string. The comparison of IRI WT and IRI C5aR2^{-/-} kidneys pointed towards differences in AKT1 and IL-10 dependent signaling (Fig. 7G). MMP and MAPkinase signaling proteins were also differentially expressed. In addition, many proteins were differentially expressed between IRI C5aR1^{-/-} and IRI C5aR2^{-/-} kidneys including AKT1, mediators of apoptosis and fibrosis, and several cytokines (Fig. 7H).

DISCUSSION

Activation of the complement system, which occurs rapidly after IRI, drives inflammation and fibrosis. The anaphylatoxin receptor C5aR has been identified to be crucial in IRI, and blocking C5aRs decreased apoptosis and inflammation^{22,23}. Until recently, C5a was thought to signal only via C5aR1. Now, a second receptor, C5aR2 (former C5L2), with functions distinct from those of C5aR1^{12,13,25,32} is recognized to be an important C5a mediator too.

In the current study, we examined the effects of 45min renal IRI which progresses to CKD within 21 days of follow up. We showed that C5aR1 and C5aR2 mRNAs quickly increased in renal tissue and remained elevated throughout the observation period of 21 days. Both C5aR1 and C5aR2 mRNAs were expressed by infiltrating immune cells and damaged proximal tubuli. We studied WT, C5aR1^{-/-}, and C5aR2^{-/-} male mice. It is worth mentioning, that complement female C57BL/6 mice show lower baseline activity of CP-C9 activity, LP-C9 activity and AP-C9 activity compared to male mice. These observations are also strain specific and are less pronounced in BALBcJ or CD1 mice³³. Both C5aR1^{-/-} and C5aR2^{-/-} mice were partially protected from IRI-induced renal inflammation and fibrosis. This is consistent with previous findings of attenuated renal damage by C5aR blockade¹¹. The protection was due to different baseline complement activation which was proven by complement activity and C3 fragment measurements³⁴. C5aR2^{-/-} IRI kidneys showed markedly better tubular regeneration with enhanced Ki-67 expression after IRI. Furthermore, the integrity of the peritubular capillary network was significantly better in C5aR2^{-/-} mice 7 and 21 days after IRI. This was confirmed

by fMRI, which revealed enhanced renal perfusion from d7 onwards in these mice. In line with previous observations, mRNA expression of the pro-inflammatory cytokine IL-1 β was reduced at d1, 7 and 21 after IRI in C5aR1 $^{-/-}$ and C5aR2 $^{-/-}$ kidneys²⁵. IL-6 expression was decreased in both C5aR deficient mouse strains. By proteomics a differential expression of anti-inflammatory IL-10 protein expression was detected and could be verified in renal tissue and in isolated BMM. In IL-10 deficient mice aggravation of IRI has been observed together with enhanced macrophage influx and decreased proliferation. These findings support an important protective role of IL-10 up-regulation in C5aR2 $^{-/-}$ IRI kidneys which might have contributed to reduced inflammation and better regeneration in our model. Our *in vitro* studies on BMM indicated that macrophages were a potential source of IL-10. IL-10 and HO-1 are interconnected by positive feedback loops and are both anti-inflammatory³⁵. HO-1 is known to have immunomodulatory properties and directs a phenotypic shift towards anti-inflammatory macrophages³⁶. Previously, we have shown that statin treatment in experimental IRI attenuated renal damage via enhanced HO-1 expression of infiltrating macrophages at the time of the injury³⁷. Enhanced HO-1 expression was not only observed in macrophages but also in the proximal tubuli of C5aR2 $^{-/-}$ mice at d1 and might have contributed to renal protection. In line with our findings in a previous study, HO-1 deficiency was linked to enhanced renal injury and up-regulated expression of the pro-inflammatory IL-6³⁸. HO-1 protects cells and tissues via antioxidative and anti-inflammatory actions. It also helps maintain microcirculation³⁹. These effects improve regeneration after IRI, and the enhanced Ki-67 $^{+}$ tubular epithelial cell numbers in C5aR2 $^{-/-}$ mice after IRI reflect this⁴⁰.

We could show *in vivo* by fMRI that the initial IRI-induced renal perfusion impairment at d1 was similar among strains. By day 7, restoration of renal perfusion was enhanced in C5aR1 $^{-/-}$ and even more in C5aR2 $^{-/-}$ mice. We have reported previously that there is a strong correlation of impaired renal perfusion at d7 after IRI and progressive renal fibrosis in mice⁴¹. Furthermore, we showed that impaired renal perfusion in patients at 14 days after kidney

transplantation correlated with decreased renal function at 12 months⁴². The better integrity of the peritubular capillary network in C5aR2^{-/-} IRI kidneys is a good explanation for the improved renal perfusion detected by fMRI and could be due to reduced inflammation. We detected an increase in AKT and p-AKT in C5aR2^{-/-} kidneys at all time points. AKT is a survival factor⁴³ and plays an important role in tissue regeneration. Moreover, studies showed that AKT is involved in HO-1 dependent pathways. In immune cells HO-1 gene expression was increased via PI3K/AKT signaling in response to prostaglandins^{44,45,46,47}. The protection from IRI induced renal fibrosis in C5aR2^{-/-} mice is striking, but unfortunately, no specific C5aR2 inhibitors are currently available. We believe that it would be useful to synthesize and test such compounds.

Taken together, this study shows distinct roles of C5aR1 and C5aR2 in a model of renal IRI with progressive renal fibrosis. Both C5aR1^{-/-} and C5aR2^{-/-} mouse strains showed attenuated inflammation and fibrosis after IRI compared to WT. By proteomic approaches a differential expression of IL-10 and AKT in C5aR2^{-/-} IRI was identified and confirmed. Along with enhanced HO-1 expression these may contribute to better regeneration of C5aR2^{-/-} IRI kidneys.

METHODS

Animals

Adult male mice (11-13 weeks of age; weight 23-28 g) were used. C5aR1^{-/-}, C5aR2^{-/-} were backcrossed more than ten generations on a C57BL/6J background and compared to WT controls. Mice were kept in a 14/10 h light/dark cycle under conventional conditions. They had free access to tap water and food (Altromin 1324). Mice were monitored daily for physical condition. The German guidelines are in accordance with the NIH guidelines for animal welfare.

Induction of renal ischemia reperfusion injury

Anesthesia was induced with isoflurane (3% induction and 1.5% maintenance). Butorphanol 1 mg/kg s.c.⁴⁸ was used for analgesia. Renal IRI was induced by left renal pedicle clamping using a micro aneurysm clip (Aesculap, Germany) for 45min. The physical condition of the mice was assessed daily. Mice were anesthetized and sacrificed by total body perfusion with ice cold PBS via the left ventricle causing circulatory arrest. The contralateral kidney was used as a control.

Magnetic resonance imaging to measure renal perfusion and kidney volume

MRI was performed on day 1, 7 and 21 after IRI using a 7 Tesla small animal scanner (Bruker, Pharmascan, PHS701, Ettlingen, Germany). Animals were anesthetized with 3% and maintained with 1-2% isoflurane, respiration was kept between 50-60 breaths per minute.

Morphological images were acquired with routine respiratory-triggered T2-weighted turbo spin echo sequences in axial and coronal planes. Kidney volumes were quantified by manual segmentation of axial images using OsiriX software (v.6.0.2; Pixmeo, Switzerland). Relative kidney volumes of the IRI kidney were given in relation to the contralateral kidney in the same animal on day 1 after IRI (the volume between d1 unclipped control and baseline did not differ). For quantitation of renal perfusion, a respiratory-triggered, fat-saturated flow-alternating inversion-recovery (FAIR) ASL-sequence with an echo-planar readout was used as described previously²⁹. This method allows contrast media free longitudinal studies of renal perfusion. Maps of renal perfusion were calculated and mean perfusion values (in ml /minute and 100 g renal tissue) of renal cortex were determined for each kidney in regions of interest. Mouse strains at the single time points were compared statistically, n=5-6 mice/group.

Renal morphology and immunohistochemistry

At day 1, 7 and 21 mice were sacrificed, kidneys fixed in 4% paraformaldehyde (PFA) and embedded in paraffin. AKI scoring was done semi-quantitatively after periodic acid Schiff (PAS) staining: 0 = focal AKI with <5% of tubuli of the cortex affected, 1 = mild AKI 5-25% of tubuli affected, 2 = moderate AKI 26-50% of tubuli affected, 3 = severe AKI 51-75% of the tubuli affected, 4 = very severe AKI > 75% of tubuli affected. To quantify renal fibrosis interstitial collagen deposition was stained by sirius red (SR)²⁹ and quantification of SR⁺ area was done automatically using Image J software (blood vessels and glomeruli were excluded). Immunohistochemistry was done to detect neutrophils (GR-1), macrophages (F4/80), tubular regeneration (Ki-67). Blinded analysis was done. Ki-67⁺ tubuli in 10 different view fields per renal section were counted at 400 fold magnification. Gr-1⁺ and F4/80⁺ leukocytes were scored semiquantitatively. 0 = <5 cells/view field (VF); 1 = mild infiltrates < 10 cells/VF, 2 = moderate infiltration 11-20 cells /VF, 3 = 21-50 cells/VF, 4 >50 cells/VF. To investigate patent peritubular capillaries (PTC) 5 min prior sacrifice 100µl tomato lectin was injected intravenously. Lectin⁺ PTC were assessed semi-quantitatively in % of the affected area in 10 view fields. PTCs in healthy kidneys were set as 100%. All images were captured with the same window size by a Keyence microscope, n=6-7 mice/group.

***In situ* RT-PCR**

Kidney paraffin sections from WT mice after IRI at 1, 7 and 21 days and controls were fixed on 3-chamber slides and developed as described previously⁴⁹. Briefly, in a two-step protocol with reverse transcription and PCR amplification, C5aR1 and C5aR2 mRNA were detected with mouse C5aR1 and C5aR2 specific primer in a specific thermal cycler. Gene specific primers for C5aR1 (Accession-N^o: NM_007577) and for C5aR2 (Accession-N^o: NM_001173550) were designed (for sequences refer to expanded methods). Detection of incorporated digoxigenin-labelled nucleotides was performed by incubation with an anti-

digoxigenin antibody labeled with alkaline phosphatase (AP). AP activity was detected by BCIP/NBT color reaction and counterstained with hematoxylin⁵⁰.

Complement activity measurement in plasma

EDTA-plasma was collected at baseline, day 1 and 7 to measure complement activation was performed as described previously³⁴. In brief, complement activation was induced by incubation of serial dilutions of plasma in ELISA plates (Nunc Maxisorp plates, Thermo Fisher Scientific) coated with human IgM, mannan and LPS to induce the classical, lectin and alternative pathway, respectively. Activation of complement was quantified at the level of C9 deposition, using a rabbit anti-mouse C9 polyclonal Ab, making it comparable to hemolytic assays. Complement activity in experimental samples was calculated using CD1 serum as a standard which was set to 100 AU/ml.

Activation of the complement system upon IRI was quantified in EDTA-plasma samples using a specific sandwich ELISA for the C3b/C3c/iC3b activation fragment, as previously described³⁴.

mRNA isolation and quantitative PCR

Kidney sections were fixed immediately after organ retrieval in RNA-later. Total RNA was extracted using the RNeasy mini kit system (Qiagen, Hilden, Germany). Then, 1µg of DNase-treated total RNA was reverse transcribed using PrimeScript Reverse Transcriptase Reagent Kit (Takara) and qPCR was performed on an Lightcycler 420 II (Roche Diagnostics, Penzberg, Germany) using FastStart Sybr-Green chemistry. The following gene-specific primers were used C5aR1, C5aR2, IL-10, IL-6, IL-1β (for details refer to expanded methods). β-actin was used as house keeper for normalization. n=5-6 mice/group.

Bone marrow derived macrophage culture and IL-10 ELISA

Bone marrow cells were isolated as previously described⁵¹. 25 ng/ml of recombinant mouse MCSF (PeproTech, Hamburg, Germany) was added to DMEM supplemented with 10% FBS, 100 U/ml penicillin, and 100 µg/ml streptomycin to differentiate bone marrow cells to macrophages. After 7 days, the differentiated macrophages were detached using accutase and plated for further experiments. For LPS stimulation, 5×10^5 cells were plated in 12 well plates and cultured overnight. Then cells were stimulated with LPS (1 µg/ml) for 16h. The supernatant collected was used for mouse IL-10 ELISA (ThermoFischer Scientific, Waltham, USA) according to the manufacturer's protocol. Cell lysates were used for protein estimation and subsequent Western blot analysis. Concentration of IL-10 measured in the supernatant was normalized to protein concentration measured in cell lysates and expressed as pg/mg protein. Cells were stained with CD206 (clone: C068C2) or the respective isotype control antibodies (Biolegend, San Diego, CA) and analyzed by flow cytometry.

Protein isolation and Western blotting

Shock frozen kidneys were re-suspended in 2 ml RIPA lysis buffer and sonificated on ice. 50 µg protein was separated on a 10% polyacrylamide gel. Proteins were transferred to PVDF membranes (Milipore, Darmstadt, Germany) and blocked in 3% BSA. Incubation in primary antibody against p-AKT (60 kDa, Ser473 D9E rabbit), AKT (56 kDa, 2H10 mouse), and 14-3-3 (28 kDa, K-19 rabbit) was applied over night at 4°C. Antibodies were from Santa Cruz Biotechnology, Dallas, USA and Cell Signaling Technologies, Cambridge, GB. After washing with TBST buffer membranes were incubated with horseradish peroxidase conjugated goat anti rabbit secondary antibody (Dianova, Hamburg, Germany) for 1 hour. Proteins were detected with SuperSignal™ West Pico Chemiluminescent Substrate (Thermo Fisher Scientific, Waltham, Massachusetts, USA) and SuperSignal™ West Femto Maximum Sensitivity Substrate (Thermo Fisher Scientific, Waltham, Massachusetts, USA) according to

the manufacturer's instructions (VersaDoc MP 400 System, Bio-Rad). Relative densities were quantified by Image J software. n=5 mice/group.

Flow cytometry

At 7 days after IRI kidneys were homogenized with a gentleMACS dissociator (Miltenyi Biotec, San Diego USA) according to manufacturer's instructions. Before and after homogenization, digestion with Collagenase II (500U/ml; Worthington) was performed. Red blood cell lysis of single cell suspensions was done in RBC lysis buffer (420301, Biolegend, San Diego). Antibody staining was performed as described previously⁵². For analysis the following anti-mouse antibodies were used: CD45 (clone 30-F11), CD49b (clone DX5), CD11c (clone N418), F4/80 (clone BM8), CD11b (clone M1/70) and fixable viability dye eFluor 506 (65-0866) from ebioscience, Santa Clara, CA. Ly6-C (clone HK1.4), Ly6G (clone 1A8) from Biolegend, San Diego, CA. FACS CantoII (BD Biosciences) was used for flow cytometry and data analysis was done using Kaluza software 1.3 (Beckmann Coulter, Krefeld), n=5 mice/ group.

High content antibody arrays

To identify differentially expressed proteins and phospho-proteins, renal tissue at d1 after IRI was shock frozen and subjected to protein isolation using scioExtract Pro (Sciomics, Germany). Protein content was measured by BCA and adjusted to 1 mg/ml. Subsequently, the protein fraction was labeled with scioDye 1 (Sciomics) and incubated for 3 hours on scioDiscover arrays (Sciomics) according to standard protocols for microarray analysis. For detection of the phosphorylation status scioPhospho detection mix (Sciomics) was added for 1 hour after washing with PBST. After washing, slides were scanned using a Powerscanner

(Tecan). Data were analyzed using the linear models for microarray data (LIMMA) package of R-Bioconductor for differential protein expression and phosphorylation status.

Statistical analysis

GraphPad prism software (GraphPad Software Inc. 5.0, San Diego, CA) was used for statistical analysis. One way ANOVA was used to compare parameters between mice strains. Adjustment for multiple comparisons was performed by a Tukey post-hoc-test. Data are presented as mean \pm standard error (SEM). Significant differences were defined as * $p < 0.05$, ** $p < 0.01$, *** $p < 0.001$.

DISCLOSURE

none

REFERENCES

1. Thadhani R, Pascual M, Bonventre JV. Acute renal failure. *The New England journal of medicine* 1996; **334**: 1448-1460.
2. McCullough JW, Renner B, Thurman JM. The role of the complement system in acute kidney injury. *Seminars in nephrology* 2013; **33**: 543-556.
3. Danobeitia JS, Djamali A, Fernandez LA. The role of complement in the pathogenesis of renal ischemia-reperfusion injury and fibrosis. *Fibrogenesis & tissue repair* 2014; **7**: 16.
4. Loirat C, Fremeaux-Bacchi V. Atypical hemolytic uremic syndrome. *Orphanet journal of rare diseases* 2011; **6**: 60.
5. Abe K, Miyazaki M, Koji T, *et al.* Enhanced expression of complement C5a receptor mRNA in human diseased kidney assessed by in situ hybridization. *Kidney international* 2001; **60**: 137-146.
6. Quigg RJ. Role of complement and complement regulatory proteins in glomerulonephritis. *Springer seminars in immunopathology* 2003; **24**: 395-410.
7. Pratt JR, Basheer SA, Sacks SH. Local synthesis of complement component C3 regulates acute renal transplant rejection. *Nature medicine* 2002; **8**: 582-587.
8. Serinsoz E, Bock O, Gwinner W, *et al.* Local complement C3 expression is upregulated in humoral and cellular rejection of renal allografts. *American journal of transplantation : official journal of the American Society of Transplantation and the American Society of Transplant Surgeons* 2005; **5**: 1490-1494.
9. Walport MJ. Complement. Second of two parts. *The New England journal of medicine* 2001; **344**: 1140-1144.
10. Walport MJ. Complement and systemic lupus erythematosus. *Arthritis research* 2002; **4 Suppl 3**: S279-293.
11. Gueler F, Rong S, Gwinner W, *et al.* Complement 5a receptor inhibition improves renal allograft survival. *Journal of the American Society of Nephrology : JASN* 2008; **19**: 2302-2312.
12. Pundir P, MacDonald CA, Kulka M. The Novel Receptor C5aR2 Is Required for C5a-Mediated Human Mast Cell Adhesion, Migration, and Proinflammatory Mediator Production. *Journal of immunology* 2015; **195**: 2774-2787.
13. Croker DE, Monk PN, Halai R, *et al.* Discovery of functionally selective C5aR2 ligands: novel modulators of C5a signalling. *Immunology and cell biology* 2016; **94**: 787-795.
14. Chenoweth DE, Goodman MG, Weigle WO. Demonstration of a specific receptor for human C5a anaphylatoxin on murine macrophages. *The Journal of experimental medicine* 1982; **156**: 68-78.

15. Chenoweth DE, Hugli TE. Demonstration of specific C5a receptor on intact human polymorphonuclear leukocytes. *Proceedings of the National Academy of Sciences of the United States of America* 1978; **75**: 3943-3947.
16. Gutzmer R, Kother B, Zwirner J, *et al.* Human plasmacytoid dendritic cells express receptors for anaphylatoxins C3a and C5a and are chemoattracted to C3a and C5a. *The Journal of investigative dermatology* 2006; **126**: 2422-2429.
17. Werfel T, Oppermann M, Schulze M, *et al.* Binding of fluorescein-labeled anaphylatoxin C5a to human peripheral blood, spleen, and bone marrow leukocytes. *Blood* 1992; **79**: 152-160.
18. Nataf S, Davoust N, Ames RS, *et al.* Human T cells express the C5a receptor and are chemoattracted to C5a. *Journal of immunology* 1999; **162**: 4018-4023.
19. Arbore G, Kemper C. A novel "complement-metabolism-inflammasome axis" as a key regulator of immune cell effector function. *European journal of immunology* 2016; **46**: 1563-1573.
20. Fayyazi A, Scheel O, Werfel T, *et al.* The C5a receptor is expressed in normal renal proximal tubular but not in normal pulmonary or hepatic epithelial cells. *Immunology* 2000; **99**: 38-45.
21. van Werkhoven MB, Damman J, Daha MR, *et al.* Novel insights in localization and expression levels of C5aR and C5L2 under native and post-transplant conditions in the kidney. *Molecular immunology* 2013; **53**: 237-245.
22. Arumugam TV, Shiels IA, Strachan AJ, *et al.* A small molecule C5a receptor antagonist protects kidneys from ischemia/reperfusion injury in rats. *Kidney international* 2003; **63**: 134-142.
23. Tuboly E, Futakuchi M, Varga G, *et al.* C5a inhibitor protects against ischemia/reperfusion injury in rat small intestine. *Microbiology and immunology* 2016; **60**: 35-46.
24. Mueller M, Herzog C, Larmann J, *et al.* The receptor for activated complement factor 5 (C5aR) conveys myocardial ischemic damage by mediating neutrophil transmigration. *Immunobiology* 2013; **218**: 1131-1138.
25. Poppelaars F, van Werkhoven MB, Kotimaa J, *et al.* Critical role for complement receptor C5aR2 in the pathogenesis of renal ischemia-reperfusion injury. *FASEB journal : official publication of the Federation of American Societies for Experimental Biology* 2017; **31**: 3193-3204.
26. Chawla LS, Bellomo R, Bihorac A, *et al.* Acute kidney disease and renal recovery: consensus report of the Acute Disease Quality Initiative (ADQI) 16 Workgroup. *Nature reviews Nephrology* 2017; **13**: 241-257.
27. Rabelink TJ, Wijewickrama DC, de Koning EJ. Peritubular endothelium: the Achilles heel of the kidney? *Kidney international* 2007; **72**: 926-930.

28. Hueper K, Peperhove M, Rong S, *et al.* T1-mapping for assessment of ischemia-induced acute kidney injury and prediction of chronic kidney disease in mice. *European radiology* 2014; **24**: 2252-2260.
29. Hueper K, Rong S, Gutberlet M, *et al.* T2 relaxation time and apparent diffusion coefficient for noninvasive assessment of renal pathology after acute kidney injury in mice: comparison with histopathology. *Investigative radiology* 2013; **48**: 834-842.
30. Schroder C, Jacob A, Tonack S, *et al.* Dual-color proteomic profiling of complex samples with a microarray of 810 cancer-related antibodies. *Molecular & cellular proteomics : MCP* 2010; **9**: 1271-1280.
31. Hoheisel JD, Alhamdani MS, Schroder C. Affinity-based microarrays for proteomic analysis of cancer tissues. *Proteomics Clinical applications* 2013; **7**: 8-15.
32. Vijayan S, Asare Y, Grommes J, *et al.* High expression of C5L2 correlates with high proinflammatory cytokine expression in advanced human atherosclerotic plaques. *The American journal of pathology* 2014; **184**: 2123-2133.
33. Kotimaa J, Klar-Mohammad N, Gueler F, *et al.* Sex matters: Systemic complement activity of female C57BL/6J and BALB/cJ mice is limited by serum terminal pathway components. *Molecular immunology* 2016; **76**: 13-21.
34. Kotimaa JP, van Werkhoven MB, O'Flynn J, *et al.* Functional assessment of mouse complement pathway activities and quantification of C3b/C3c/iC3b in an experimental model of mouse renal ischaemia/reperfusion injury. *Journal of immunological methods* 2015; **419**: 25-34.
35. Ryter SW, Choi AM. Heme oxygenase-1: molecular mechanisms of gene expression in oxygen-related stress. *Antioxidants & redox signaling* 2002; **4**: 625-632.
36. Naito Y, Takagi T, Higashimura Y. Heme oxygenase-1 and anti-inflammatory M2 macrophages. *Archives of biochemistry and biophysics* 2014; **564**: 83-88.
37. Gueler F, Park JK, Rong S, *et al.* Statins attenuate ischemia-reperfusion injury by inducing heme oxygenase-1 in infiltrating macrophages. *The American journal of pathology* 2007; **170**: 1192-1199.
38. Tracz MJ, Juncos JP, Croatt AJ, *et al.* Deficiency of heme oxygenase-1 impairs renal hemodynamics and exaggerates systemic inflammatory responses to renal ischemia. *Kidney international* 2007; **72**: 1073-1080.
39. Zhang FH, Sun YH, Fan KL, *et al.* Protective effects of heme oxygenase-1 against severe acute pancreatitis via inhibition of tumor necrosis factor-alpha and augmentation of interleukin-10. *BMC gastroenterology* 2017; **17**: 100.
40. Nguan CY, Guan Q, Gleave ME, *et al.* Promotion of cell proliferation by clusterin in the renal tissue repair phase after ischemia-reperfusion injury. *American journal of physiology Renal physiology* 2014; **306**: F724-733.

41. Hueper K, Hartung D, Gutberlet M, *et al.* Magnetic resonance diffusion tensor imaging for evaluation of histopathological changes in a rat model of diabetic nephropathy. *Investigative radiology* 2012; **47**: 430-437.
42. Hueper K, Gueler F, Brasen JH, *et al.* Functional MRI detects perfusion impairment in renal allografts with delayed graft function. *American journal of physiology Renal physiology* 2015; **308**: F1444-1451.
43. Curci C, Castellano G, Stasi A, *et al.* Endothelial-to-mesenchymal transition and renal fibrosis in ischaemia/reperfusion injury are mediated by complement anaphylatoxins and Akt pathway. *Nephrology, dialysis, transplantation : official publication of the European Dialysis and Transplant Association - European Renal Association* 2014; **29**: 799-808.
44. Ryter SW, Alam J, Choi AM. Heme oxygenase-1/carbon monoxide: from basic science to therapeutic applications. *Physiological reviews* 2006; **86**: 583-650.
45. Wijayanti N, Kietzmann T, Immenschuh S. Heme oxygenase-1 gene activation by the NAD(P)H oxidase inhibitor 4-(2-aminoethyl) benzenesulfonyl fluoride via a protein kinase B, p38-dependent signaling pathway in monocytes. *The Journal of biological chemistry* 2005; **280**: 21820-21829.
46. Martin D, Rojo AI, Salinas M, *et al.* Regulation of heme oxygenase-1 expression through the phosphatidylinositol 3-kinase/Akt pathway and the Nrf2 transcription factor in response to the antioxidant phytochemical carnosol. *The Journal of biological chemistry* 2004; **279**: 8919-8929.
47. Alvarez-Maqueda M, El Bekay R, Alba G, *et al.* 15-deoxy-delta 12,14-prostaglandin J2 induces heme oxygenase-1 gene expression in a reactive oxygen species-dependent manner in human lymphocytes. *The Journal of biological chemistry* 2004; **279**: 21929-21937.
48. Gueler F, Shushakova N, Mengel M, *et al.* A novel therapy to attenuate acute kidney injury and ischemic allograft damage after allogenic kidney transplantation in mice. *PloS one* 2015; **10**: e0115709.
49. Jorns A, Gunther A, Hedrich HJ, *et al.* Immune cell infiltration, cytokine expression, and beta-cell apoptosis during the development of type 1 diabetes in the spontaneously diabetic LEW.1AR1/Ztm-iddm rat. *Diabetes* 2005; **54**: 2041-2052.
50. Jorns A, Arndt T, Meyer zu Vilsendorf A, *et al.* Islet infiltration, cytokine expression and beta cell death in the NOD mouse, BB rat, Komeda rat, LEW.1AR1-iddm rat and humans with type 1 diabetes. *Diabetologia* 2014; **57**: 512-521.
51. Zhang X, Goncalves R, Mosser DM. The isolation and characterization of murine macrophages. *Current protocols in immunology* 2008; **Chapter 14**: Unit 14 11.
52. Klemann C, Schroder A, Dreier A, *et al.* Interleukin 17, Produced by gammadelta T Cells, Contributes to Hepatic Inflammation in a Mouse Model of Biliary Atresia and Is Increased in Livers of Patients. *Gastroenterology* 2016; **150**: 229-241 e225.

ACKNOWLEDGMENT

We thank Herle Chlebusch, Michaela Beese, Robert Laudely and Christian Bergen (MHH) for excellent technical assistance. We thank Iuliia Kotovafor and Florian Skwirblies at Sciomics for protein work up. We thank Craig Gerard (Harvard University, Boston, USA) for the breeding pairs of C5aR2^{-/-} mice. We thank Michael Brownstein for editing the manuscript. This work was supported by the Federal Ministry of Education and Research (BMBF; grant 01FP09104C to F.G.) and by the German Science Foundation (Deutsche Forschungsgemeinschaft; DFG; grants GU 613/1-1 to FG, and HU- to KH) HU2232/1-1 and KL603/10-1 (AK).

FIGURE LEGENDS

Figure 1: C5aR1 and C5aR2 mRNA expression increases after renal IRI

Following IRI, C5aR1 (A) and C5aR2 (B) mRNA levels were significantly upregulated at all time points studied compared to levels in control kidneys (n=5-6, β -actin was used for normalization, mean \pm SEM ***p < 0.001). Complement activity was measured at baseline in EDTA plasma of WT, C5aR1^{-/-} and C5aR2^{-/-} mice. Activity of the classical (CP), alternative (AP) and the mannose-binding lectin pathway (LP) did not differ between groups (C, n=6-8 per group). C3 fragmentation was measured by ELISA and was enhanced at d1 after IRI in all groups (D). In situ RT-PCR for C5aR1 (upper row), and C5aR2 (lower row) mRNA expression was done at day 1, 7 and 21 after IRI in WT kidneys. After IRI expression of C5aR1 and C5aR2 mRNA especially in the parenchymal cells of the proximal tubuli (star) were markedly increased from a moderate expression at day 7 (F, J) to a high, dense expression at day 21 (G, K). Additionally, the immune cell infiltration (arrow), starting at day 1 only in the perivascular space of some greater vessels and reaching a severe infiltration at day 21, showed a dense mRNA expression of both receptors (bar 50 μ m).

Figure 2: Myeloid cell infiltration is reduced in C5aRs deficient IRI kidneys at d1 and d7

Myeloid cell infiltration was attenuated in C5aR-deficient mice after IRI. In WT mice Gr-1⁺ neutrophils (red) accumulated in the outer medulla at d1 after IRI. C5aR1^{-/-} and C5aR2^{-/-} IRI kidneys showed significantly reduced Gr-1⁺ neutrophil accumulation (left column). The effect was greater in C5aR2^{-/-} animals. Seven days after IRI, F4/80⁺ macrophages (red) were the predominant cells in the outer medulla. Again, kidneys of C5aR1^{-/-} mice and, to a greater degree, C5aR2^{-/-} mice had attenuated F4/80⁺ macrophage infiltration (middle column, magnification: 200x). Flow cytometry at d7 after IRI confirmed the attenuated CD11b⁺/F4/80⁺ macrophage infiltration in C5aR1^{-/-} and C5aR2^{-/-} IRI kidneys compared to WT (C gating, F quantification). *In vivo* lectin staining revealed enhanced loss of in PTCs in WT IRI kidneys at d7 compared to C5aR2^{-/-} or C5aR1^{-/-} IRI kidneys (N, bar 100µm, mean±SEM. *p < 0.05, **p < 0.01, ***p < 0.001 for C5aR2^{-/-} and C5aR1^{-/-}). At d1 the PTC patency rate was not yet reduced (K).

Figure 3: Cytokine, IL-10 and HO-1 expression after IRI

IL-1β mRNA increase was attenuated in C5aR1^{-/-} and C5aR2^{-/-} IRI kidneys compared to WT (A-C). IL-6 mRNA up-regulation was similar at d1 in all groups but significantly less at d7 in C5aR1^{-/-} and C5aR2^{-/-} IRI kidneys (D-F). The anti-inflammatory IL-10 mRNA was up-regulated in C5aR2^{-/-} IRI kidneys at day 1, 7 and 21 (G-I; mean± SEM, *p < 0.05, **p < 0.01 n=6-8 per group). Immunohistochemistry revealed significantly more HO-1 expression in C5aR2^{-/-} proximal tubuli at d1 compared to WT at d1 after IRI. C5aR1^{-/-} IRI kidneys did not differ from WT. (J-L: bar 100µm, mean±SEM. **p < 0.01).

BMM from C5aR2^{-/-} mice showed enhanced IL-10 production after LPS stimulation compared to WT (M). Western Blot revealed enhanced HO-1 expression in C5aR2^{-/-} derived BMM after stimulation (N). Flow cytometry showed enhanced expression of CD 206 in C5aR2^{-/-} derived

BMM compared to WT after stimulation (mean±SEM, *p < 0.05 experiments were repeated 3 times).

Figure 4: C5aR-deficient IRI kidneys have less renal injury and inflammation at d21

Acute kidney injury (AKI) was enhanced in IRI kidneys of WT mice compared to control at d21 after IRI (PAS stain, first column with AKI score). In C5aR1^{-/-} and especially C5aR2^{-/-} IRI kidneys AKI was significantly attenuated compared to WT at d21. Control kidneys displayed no signs of AKI (J). WT IRI kidneys showed persistent increased F4/80⁺ macrophage infiltration (red) at d21 (middle column). C5aR1^{-/-} IRI kidneys had significantly less F4/80⁺ macrophage infiltration. In C5aR2^{-/-} IRI kidneys the macrophage accumulation was only focal. Lectin staining revealed enhanced loss of patent peritubular capillaries (PTC) in WT IRI kidneys at d21 (last column). C5aR2^{-/-} IRI kidneys had markedly enhanced patent PTCs compared to WT. To a minor degree also C5aR1^{-/-} IRI kidneys had larger proportion of patent PTC (bar 100µm, mean±SEM. *p < 0.05, **p < 0.01, ***p < 0.001 for C5aR2^{-/-} and *p for C5aR1^{-/-}).

Figure 5: C5aR2^{-/-} mice had significantly better renal perfusion after IRI

Representative parameter maps of renal perfusion generated from fMRI (arterial spin labelling, ASL) of the IRI kidney are shown in WT (upper row), C5aR1^{-/-} (middle row) and C5aR2^{-/-} mice (lower row) at d1, 7 and 21 (A). For comparison, the contralateral kidney on d1 served as a reference control (left lower corner, A). Quantification of perfusion values is depicted as mean+SEM and was calculated per 100g renal tissue (B). On d1 after IRI, perfusion was mildly impaired in all groups compared to the contralateral control kidney. From d7 onwards, C5aR1^{-/-} and even more C5aR2^{-/-} mice showed significantly improved perfusion compared to WT mice at d7 and d21 (B; C5aR2^{-/-} vs WT *p<0.05, **p<0.01, C5aR1^{-/-} vs WT *p<0.05). Better perfusion also resulted in improved glomerular filtration rate measured by inulin clearance after contralateral nephrectomy in C5aR2^{-/-} > C5aR1^{-/-} IRI kidneys compared to WT at d21 (C,

mean±SEM. C5aR2^{-/-} vs WT: **p < 0.01, ***p < 0.001, C5aR1^{-/-} vs WT: *p<0.05).

Figure 6: Renal fibrosis and kidney volume loss were attenuated in C5aR2^{-/-} IRI kidneys 21 days after IRI

Collagen deposition (sirius red) was markedly reduced in C5aR2^{-/-} compared to WT IRI kidneys at d21 and almost comparable to sham (sham, A, Keyence Z stack; IRI second column, bar 100µm). By morphometric MRI at the volume of the IRI kidney d21 was compared to the volume of the control kidney (contralateral kidney on d1, F) to calculate the relative kidney volume. Volume loss at d21 was attenuated in C5aR2^{-/-} IRI kidneys compared to WT (last column).

Figure 7: C5aR2^{-/-} kidneys after IRI had more Ki-67⁺ tubular epithelial cells and enhanced AKT expression and activation

Enhanced numbers of Ki-67⁺ tubular epithelial cell nuclei (red) were observed in C5aR2^{-/-} IRI kidneys at d1 and 7 representing enhanced proliferation (A: C5aR2^{-/-} IRI d1; bar 50µm, B: quantification, mean ± SEM. *p < 0.05, **p < 0.01, ***p < 0.001). Western blotting (C) revealed higher AKT protein and abundance and phosphorylation in C5aR2^{-/-} IRI kidneys (D-E, normalization to 14-3-3, F normalization p-AKT/AKT; three representative samples are shown in each group and n=5-6 kidneys per group were compared, mean ± SEM *p < 0.05, **p < 0.01, ***p < 0.001). Differentially expressed proteins between WT and C5aR2^{-/-} (G) and between C5aR1^{-/-} and C5aR2^{-/-} (H) IRI kidneys at d1 revealed strong evidence for AKT1 and IL-10 signaling dependent mechanisms (STRING pathway analysis tool).

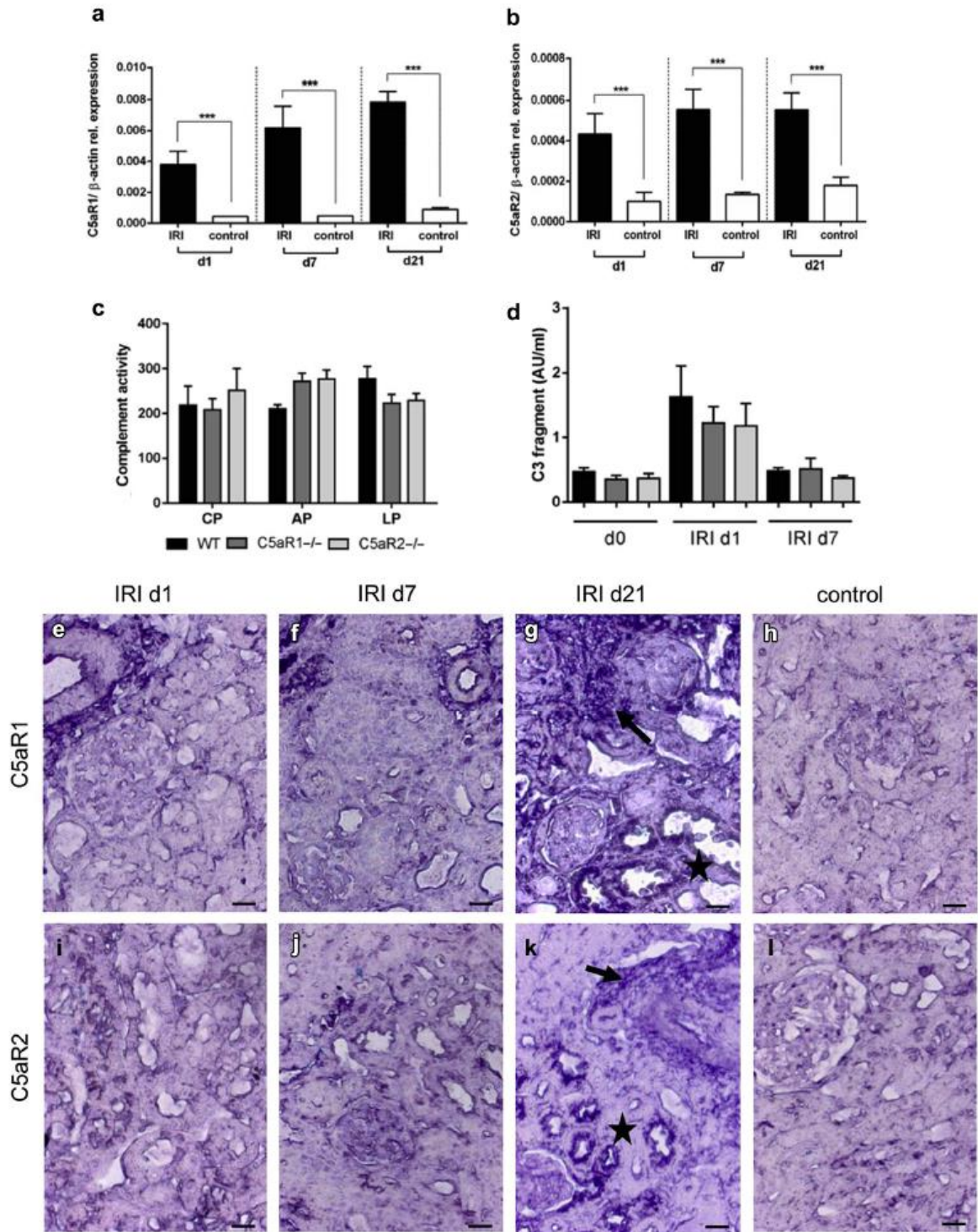


Figure 1

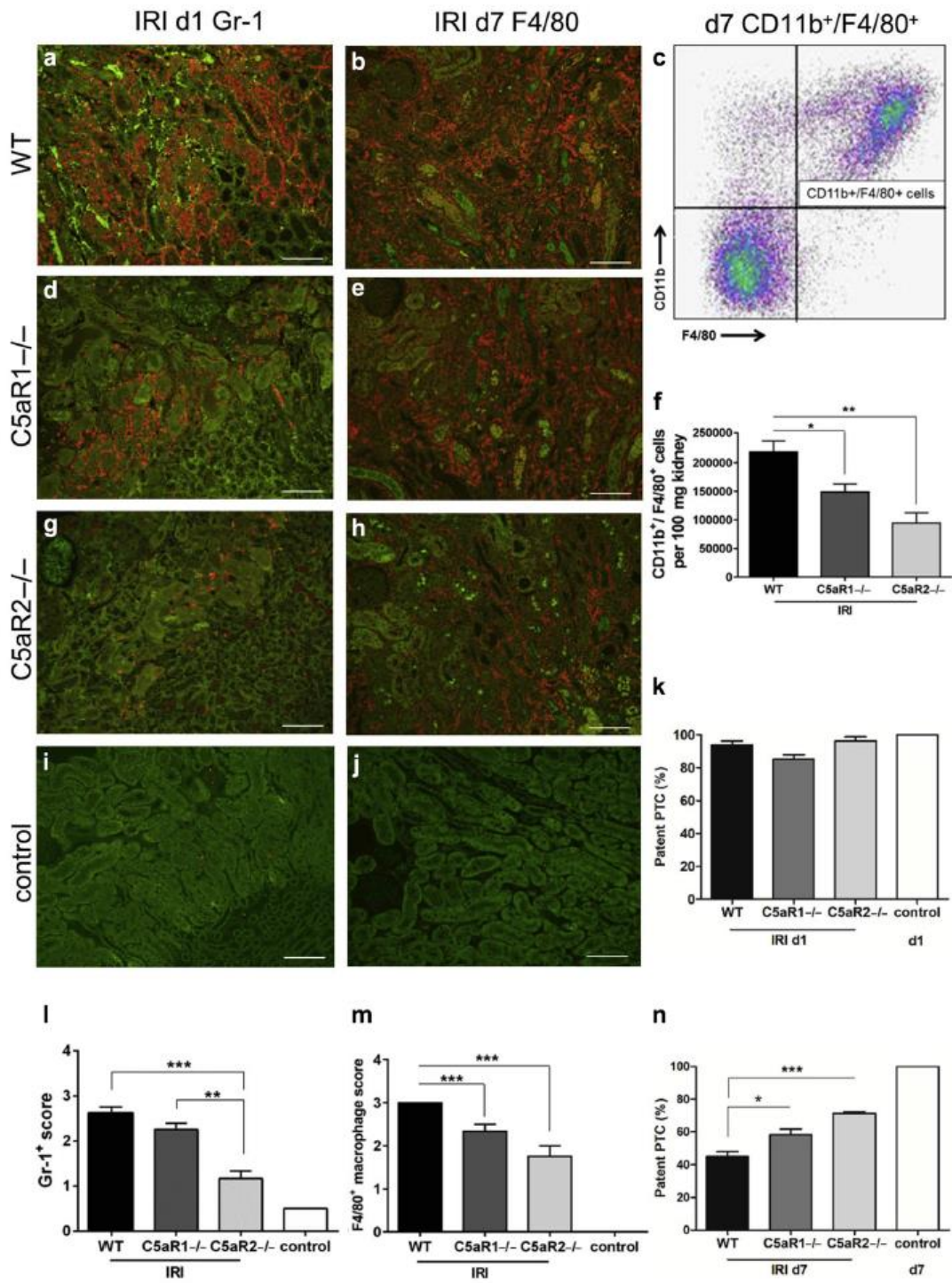


Figure 2

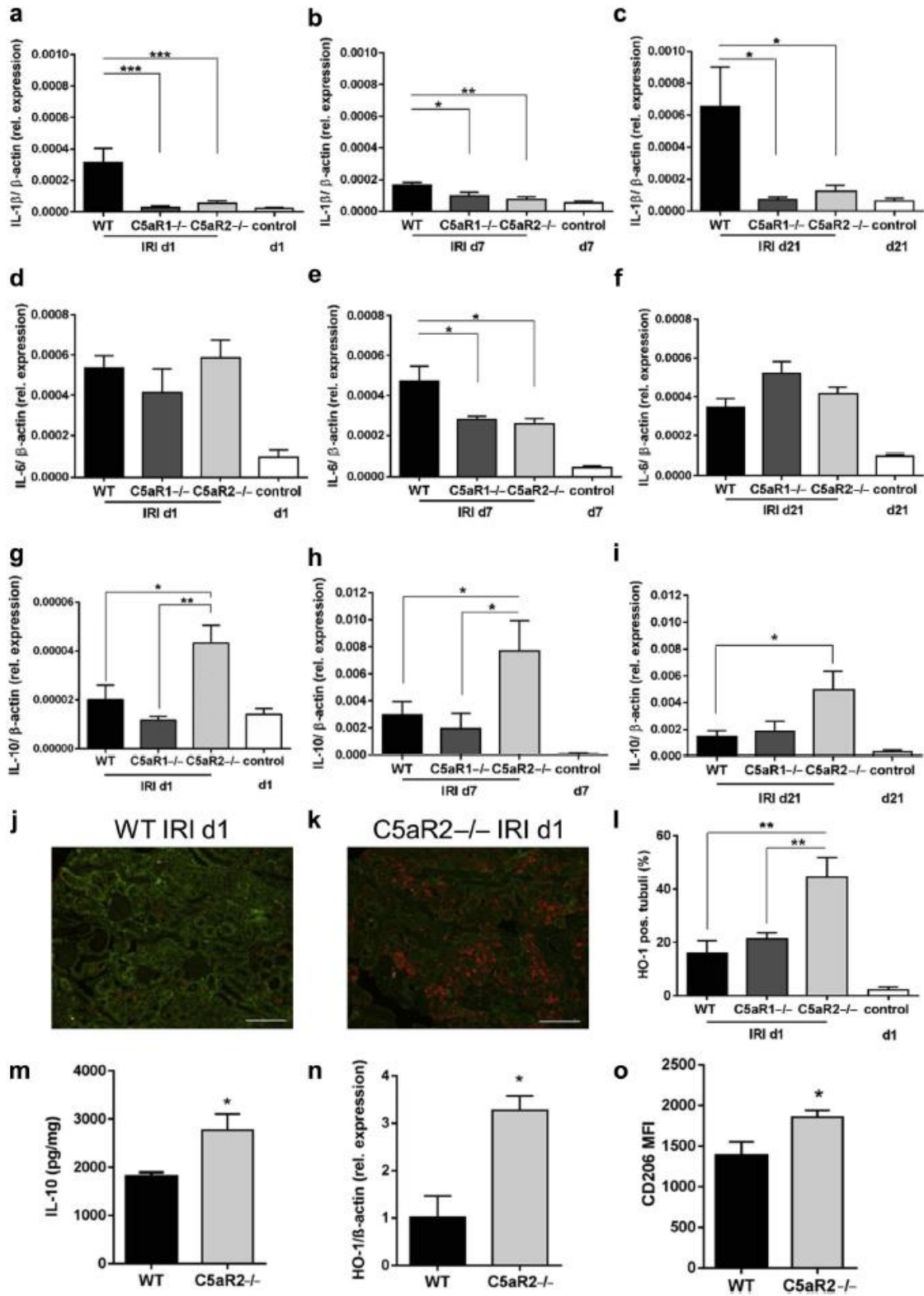


Figure 3

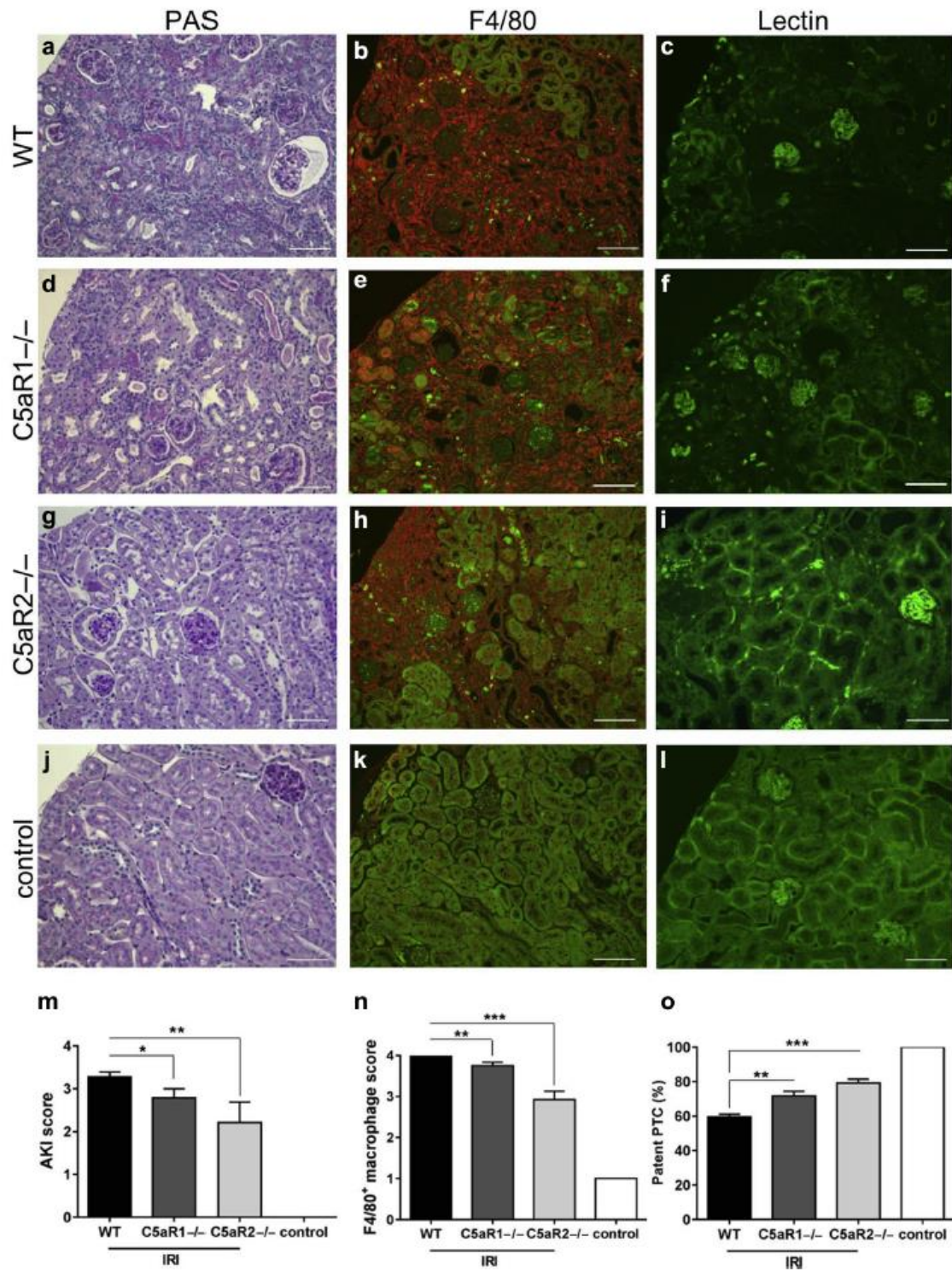
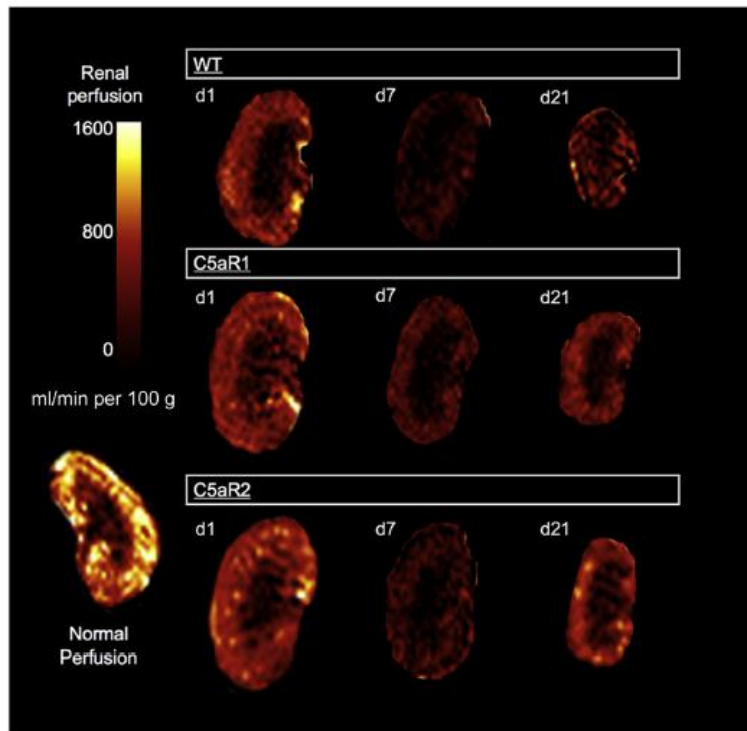


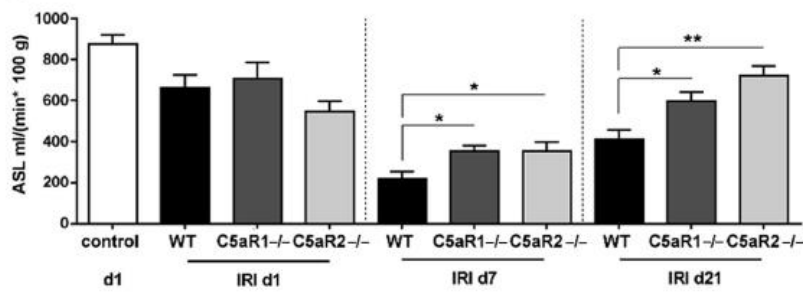
Figure 4

a

Arterial Spin Labeling (ASL)



b



c

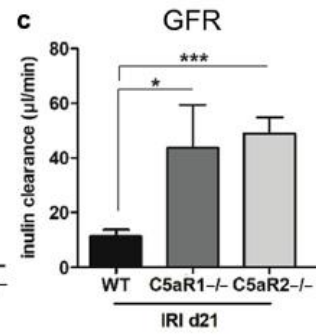


Figure 5

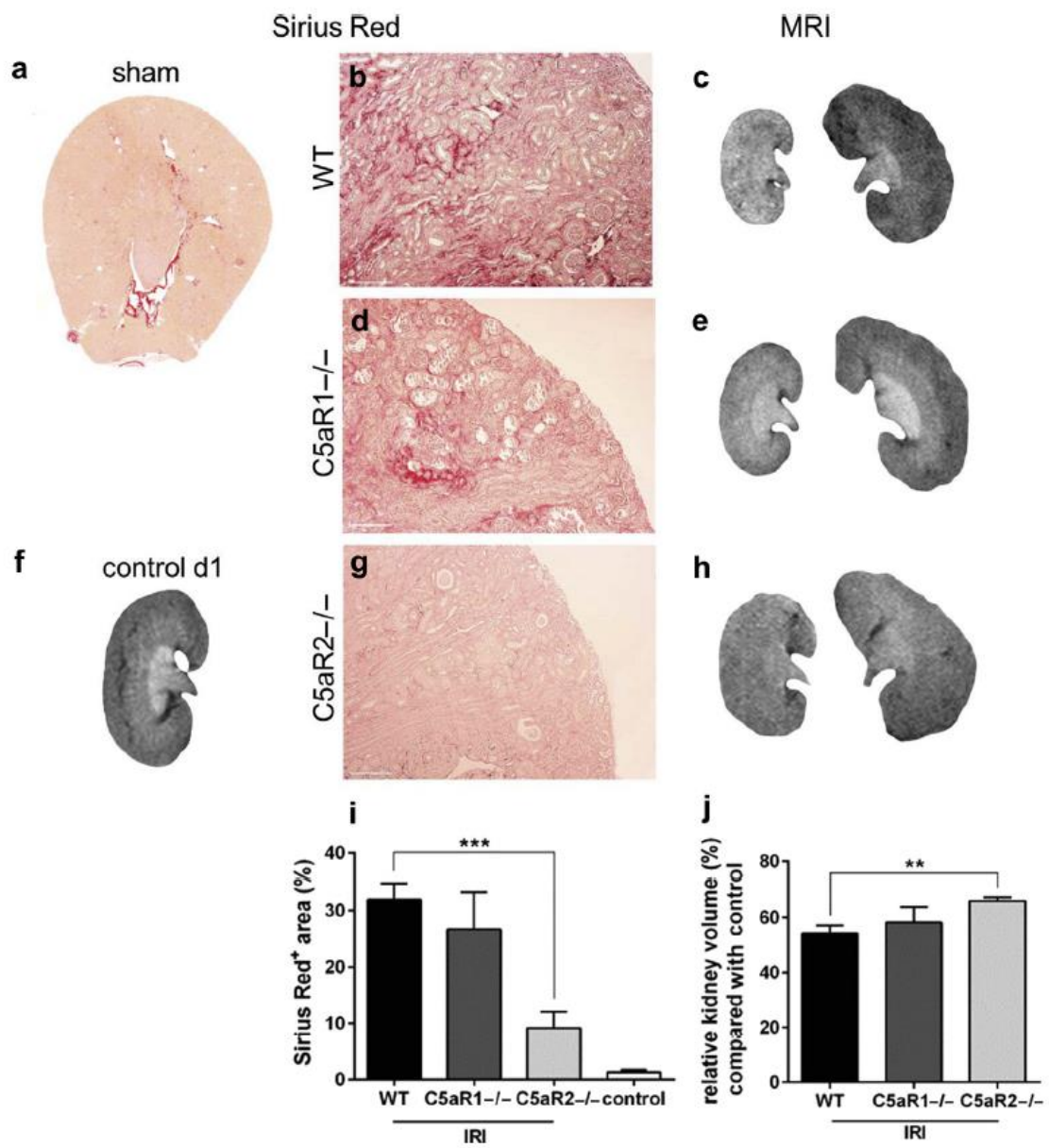


Figure 6

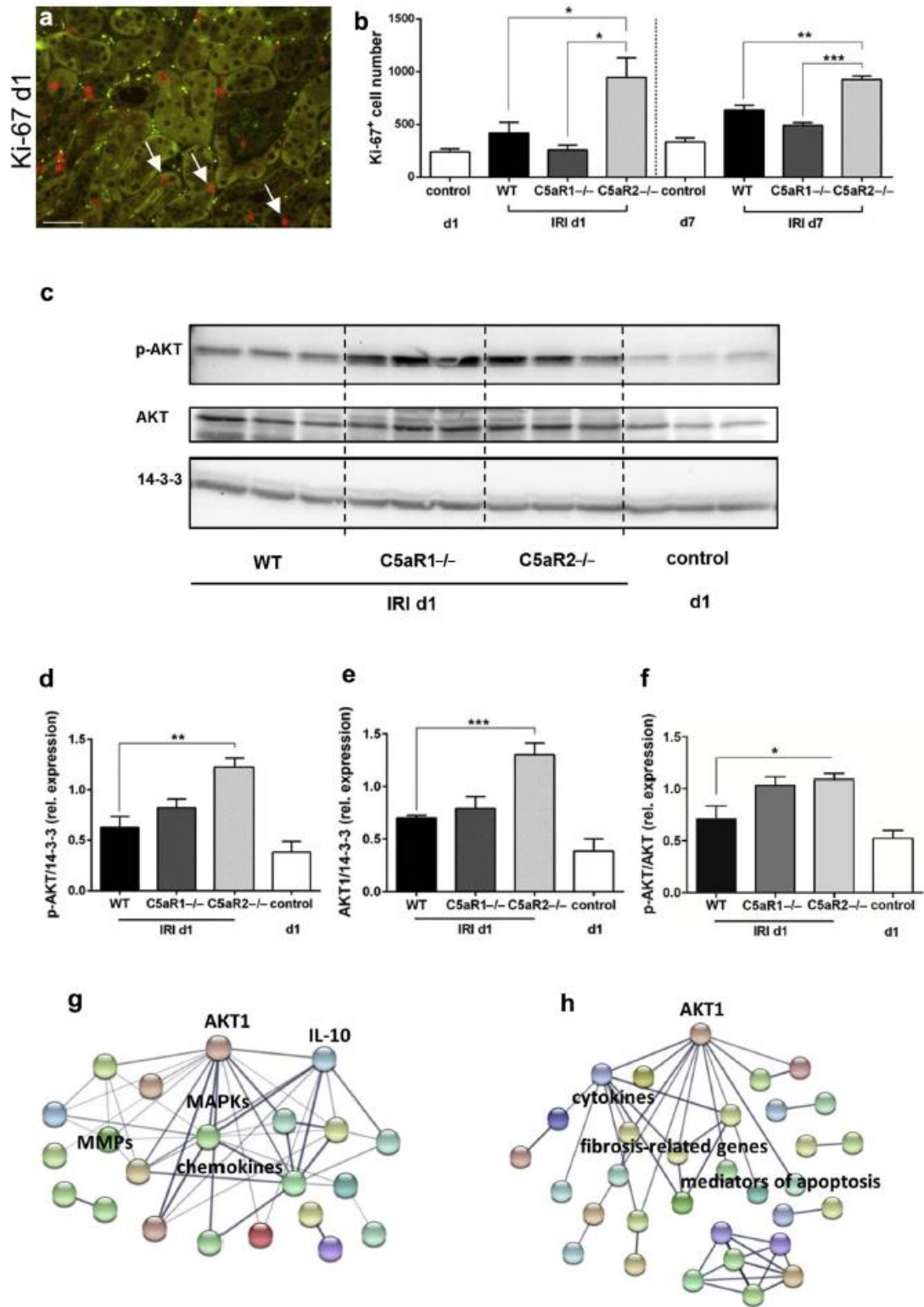


Figure 7